Progress In Electromagnetics Research Letters, Vol. 31, 1–13, 2012

ANALYTICAL STUDY OF WIDE-BAND BANDPASS FILTERS BASED ON WIRE-BONDED MULTICONDUCTOR TRANSMISSION LINES WITH LH BEHAVIOUR

J. J. Sánchez-Martínez* **and E. Márquez-Segura**

Departamento de Ingeniería de Comunicaciones, Escuela Técnica Superior de Ingeniería de Telecomunicación, Campus de Teatinos, Málaga 29071, Spain

Abstract—This paper presents a design methodology of wide-band bandpass filters based on short-circuited multi-conductor transmission lines with bonding wires between alternated strips. General design guidelines, based on analytical equations, are derived and a left-handed behaviour of the multiconductor structure is inferred and studied. Analytical equations are assessed by means of full-wave electromagnetic simulations and experimental work. A very good agreement between theoretical results and measurements is achieved, that allows both the design and performance analysis of filters without the need for costly electromagnetic simulations. In addition, the equations presented yield a compact design of the filter with a left-handed behavior.

1. INTRODUCTION

Nowadays, with the development of broadband communication systems, bandpass filters play an important and crucial role. At the transmitter side, filters are used to guarantee the transmitted signal meets a particular power spectral density mask, and at the receiver side, to eliminate the out-of-band noise. In this sense, bandpass filters, based on the transmission line approach of left-handed materials [1], have been presented in [2–6].

Realizations of composite right/left handed (CRLH) transmission lines by means of structures consisting of series capacitors and shunt inductors have been reported using different topologies and geometrical models, where the right handed behavior is consequence of parasitic

Received 25 January 2012, Accepted 28 February 2012, Scheduled 4 April 2012

* Corresponding author: Juan José Sánchez-Martínez (jjsm@ic.uma.es).

series inductor and shunt capacitor [7]. Besides, the design of such structures normally relies on electromagnetic simulations to calculate their proper dimensions.

Therefore, in this paper, the analytical design of a bandpass filter with left handed (LH) behaviour is given. The use of coupled lines to design artificial CRLH transmission lines are given in [8–10]. Here, the unit cell used to synthesize the bandpass filter consists of a short-circuited wire-bonded multiconductor transmission line (MTL) (Fig. 1). This element, when simplified to a pair of coupled lines, can be found in [11–13], but focused on the magnitude of its frequency response. However, the approach here is different. On the one hand, the analysis is extended to multi-conductor structures, and thus, the number of strips can be higher than two. On the other hand, we are interested in the magnitude of the frequency response (insertion and return losses), but also in the phase (dispersion curve) of the filter. Furthermore, the theory developed in this work, where the MTL is fully characterized by means of analytical equations, can be applied for other structures as those given in [14–16], as well as the rat-race coupler shown in [17]. In addition, by means of the proposed unit cell, some prototypes are fabricated and measured.

2. THEORY AND DESIGN

2.1. Theory

The layout of the proposed unit cell, consisting of a wire-bonded multiconductor MTL with two of its ports short-circuited to ground, is shown in Fig. 1. This two-port device can be characterized using the four-port admittance matrix given in [18] and imposing the short-circuit condition. Thus, if the MTL is assumed to be lossless, the following admittance matrix is obtained

$$[Y] = \frac{1}{\sin\theta_c}\begin{bmatrix} -jM\cos\theta_c & jN \\ jN & -jM\cos\theta_c \end{bmatrix}, \tag{1}$$

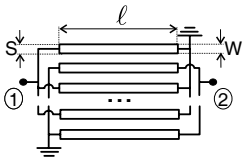

Figure 1. Structure of the proposed unit cell consisting of a short-circuited wire-bonded MTL.

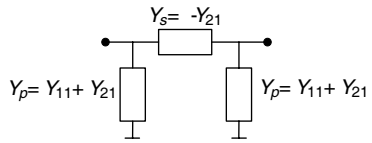

Figure 2. $\prod$-type two-port circuit.

where θ_c is the electrical length of the conductors, and M and N are defined by [18]

$$M = \frac{k}{2}Y_{11} + \left(\frac{k}{2} - 1\right)\frac{Y_{12}^2}{Y_{11}}, \quad N = (k-1)Y_{12}. \tag{2}$$

Admittances Y_{11} and Y_{12} are calculated as

$$Y_{11} = \frac{1}{2}\left(Y_{oo} + Y_{oe}\right), \quad Y_{12} = -\frac{1}{2}\left(Y_{oo} - Y_{oe}\right), \tag{3}$$

where Y_{oo} and Y_{oe} are the odd and even modes admittances respectively, of a pair of adjacent lines and k relates to the number of lines for conductors. When no losses are considered Y_{oo} and Y_{oe} are real numbers and $M > 0$, $N < 0$ and $M^2 > N^2$.

Furthermore, using matrix (1), parameters of Π equivalent circuit of a two-port circuit shown in Fig. 2, can be computed as

$$Y_s = -jN\csc\theta_c \tag{4a}$$

$$Y_p = j\left(N\csc\theta_c - M\cot\theta_c\right). \tag{4b}$$

Considering (4), it is straightforward to analyze the frequency responses of both admittances, Y_s and Y_p. An example of such admittances is shown in Fig. 3. As seen, the series admittance pass from capacitance to inductance at $\theta_c = \pi$, and the behavior of the shunt admittance is conditioned by the same singularity and two zeros, θ_{z_1} and θ_{z_2}, respectively. By operating on (4b), θ_{z_1} can be expressed as

$$\theta_{z_1} = \arccos\left(\frac{N}{M}\right) = \arccos\left(\frac{(k-1)(1-u^2)}{2u+(k-1)(1+u^2)}\right), \tag{5}$$

where $u = Z_{oe}/Z_{oo}$ and $\theta_{z_2} = 2\pi - \theta_{z_1}$. Therefore, the different operating bands are clearly defined by

$$\theta_c \in \begin{cases} (0, \theta_{z_1}) & \text{LH Band} \\ [\theta_{z_1}, \theta_{z_2}] & \text{Stop-band} \\ (\theta_{z_2}, 2\pi) & \text{RH Band} \end{cases}. \tag{6}$$

Furthermore, using the expression for the coupling coefficient c of a quarter-wavelength k-line coupler, given as [19]

$$c = \frac{(k-1)(u^2-1)}{2u + (k-1)(u^2+1)}, \tag{7}$$

it is easy to verify that

$$\theta_{z_1} = \arccos\left(-c\right), \tag{8}$$

what establishes a simple and direct relation between the left-handed bandwidth and the coupling coefficient.

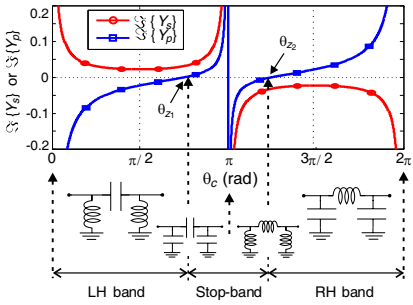

Figure 3. ℑExample of imaginary part of Y_s and Y_p admittances of a short-circuited wire-bonded MTL.

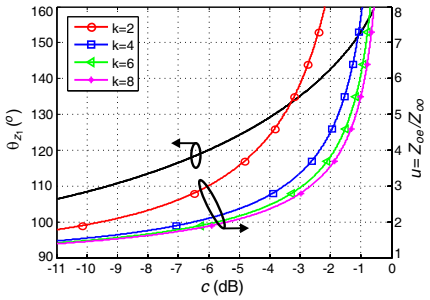

Figure 4. θ_{z1} and u as a function of the coupling factor for several number of strips k.

By means of (5) and (8), Fig. 4 represents θ_{z_1} and u as a function of the coupling coefficient c for several number of conductors k. As shown, as the lines become more tightly coupled both, θ_{z_1} and u raise. Furthermore, for a particular value of c, the greater k, the lower the value of u. In addition, increasing the number of strips allows using a lower $u = Z_{oe}/Z_{oo}$ ratio to achieve a particular LH bandwidth, which is directly related to greater widths W and spacing S between conductors. This implies to relax the manufacturing process and obtain wider dimensions for practical microstrip fabrication.

Cascading the short-circuited wire-bonded MTL of Fig. 1, the propagation constant $\gamma\ell = (\alpha + j\beta)\ell$ of the resulting periodic structure can be calculated as [20]

$$\cosh\gamma\ell = \frac{\sqrt{Y_{11}Y_{22}}}{Y_{21}} = \frac{M}{N}\cos\theta_c, \tag{9}$$

that can be simplified to

$$(\alpha + j\beta)\ell = \alpha\ell + j\theta = \cosh^{-1}\left(-\frac{\cos\theta_c}{c}\right). \tag{10}$$

From this expression, the stop-bands are clearly identified as the frequencies where $|\cos\theta_c/c| > 1$ and thus, where the propagation constant pass from being pure imaginary to pure real.

Furthermore, by simple transformations of (1) [20], the S_{11} and S_{21} parameters can be expressed as

$$S_{11} = \frac{Z_0^2 + K^2P}{D} \qquad S_{21} = -j\frac{2KNZ_0}{D}, \tag{11}$$

where Z_0 is the reference impedance and the variables P, K and D are given by

$$P = M^2 \cos^2 \theta_c - N^2 \tag{12a}$$

$$K = \frac{\sin \theta_c}{P} \tag{12b}$$

$$D = K^2 P - Z_0^2 - j2KZ_0 M \cos \theta_c. \tag{12c}$$

2.2. Design

By means of (10) and (11) both, the magnitude and phase of the frequency response of the bandpass filter, can be easily evaluated. Nevertheless, although by means of these expressions the MTL is characterized, further analysis is desired to get a better control on the performance of the structure.

The image impedance of the wire-bonded multiconductor TL can be calculated as [20]

$$\frac{Z_I}{Z_0} = \left(\frac{\sin^2 \theta_c}{N^2 - M^2 \cos^2 \theta_c} \right)^{1/2}, \tag{13}$$

that allows the calculation of the required even and odd mode impedances as

$$\frac{Z_{oe}}{Z_0} = \left| \frac{u(k-1+u)(1+(k-1)u))}{(1+u)^2} \csc^2 \theta_o - \frac{\left(2u+(k-1)(1+u^2)\right)^2}{4(1+u)^2} \right|^{1/2} \tag{14a}$$

$$Z_{oo} = Z_{oe}/u, \tag{14b}$$

where θ_o stands for the electrical length where S_{11}=0.

Figure 5 shows the magnitude of S_{11} (11) as a function of u and θ_c for $k = 2$, using as design parameters $\theta_o = 90°$ (Fig. 5(a)) and $\theta_o = 70°$ (Fig. 5(b)), respectively. By inspection of both figures, it is seen that depending on θ_o there is one or two electrical lengths where the matching is ideal and that the higher the value of u, the broader the operating frequency band. This property is most noticeable in Fig. 6 where curves are particularized for only two values of u.

Therefore, by increasing u the operating bandwidth broadens and, according to Fig. 4, the LH-band also extends. Besides, as seen in Fig. 4, the higher the number of conductors, the less stringent is the coupling coefficient for a particular value of u.

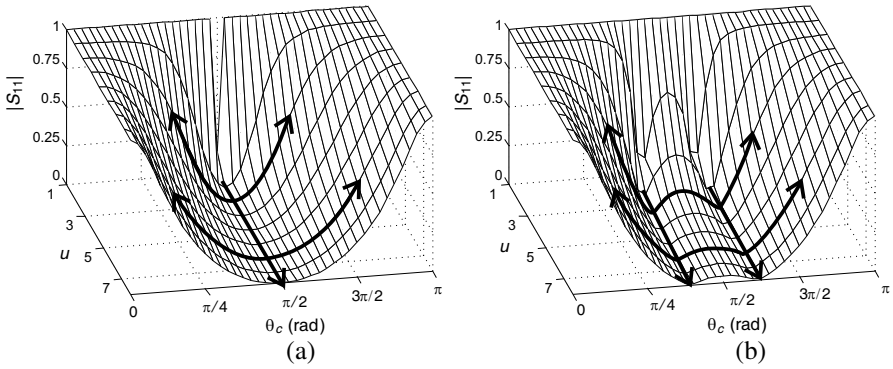

Figure 5. Magnitude of S_{11} (11) as a function of $u = Z_{oe}/Z_{oo}$ and θ_c for $k = 2$. (a) $\theta_o = 90°$ and (b) $\theta_o = 70°$.

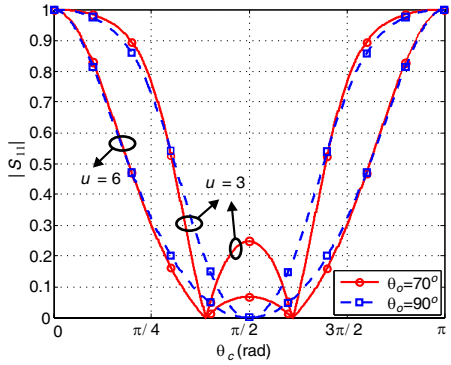

Figure 6. $|S_{11}|$ versus θ_c for $k = 2$, $u = [3, 6]$, and $\theta_o = [70°, 90°]$.

Consequently, for each value of u and k, there is a pair of values of Z_{oe} and Z_{oo} to obtain perfect match at a particular θ_o. If $\theta_o = 90°$, (14) can be simplified as

$$\frac{Z_{oe}}{Z_0} = \frac{(k-1)(u-1)}{2}, \tag{15}$$

that is equivalent to the equation given in [13] as

$$\frac{Z_{oe}}{Z_0} = \frac{c}{1-c} \tag{16}$$

to calculate the even mode impedance as a function of the coupling coefficient when the termination impedances at both sides of the multiconductor element are equal to Z_0 and $k = 2$. Nevertheless, it is important to highlight that (16) is only valid for $k = 2$ and $\theta_o = 90°$.

Furthermore, it can be proved that when the same coupling factor is considered, the S-parameters are equal regardless the value of k. Fig. 7 depicts the standing wave ratio (SWR) for several coupling factors and two θ_o, 90° and 70°. These curves, as mentioned before, do not depend on k and show how increasing the coupling value the operating band broadens. Besides, as expected, the matching is perfect at θ_o, and for $\theta_o \neq 90°$, the lower the coupling factor, the greater the mid-band SWR at $\theta_c = 90°$.

Once the magnitude of the frequency response of the multiconductor structure has been analyzed, Fig. 8 depicts, by means of (10), the dispersion of a lossless unit cell for several coupling levels. As seen, by increasing the coupling value the slope of θ decreases. Besides, it is important to remark that these curves do not depend on neither k nor θ_o.

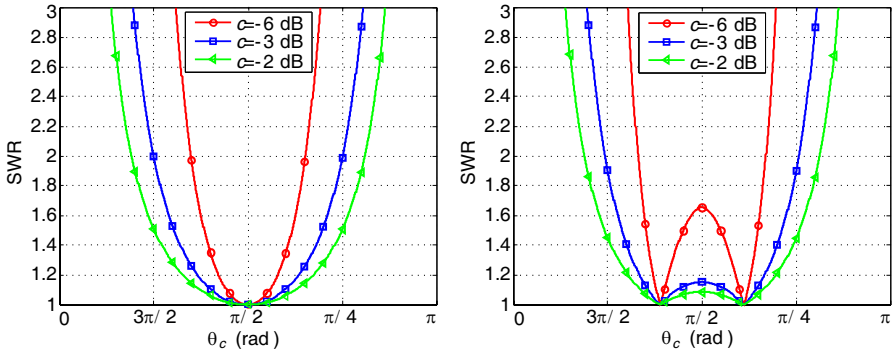

Figure 7. SWR as a function of θ_c for several coupling factors. (a) $\theta_o = 90°$ and (b) $\theta_o = 70°$.

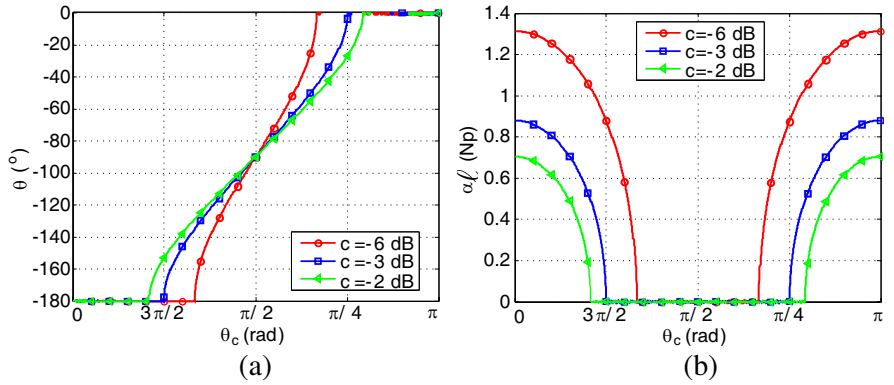

Figure 8. (a) $\theta = \beta\ell$ and (b) $\alpha\ell$ as a function of θ_c for several coupling factors. These curves do not depend neither k nor θ_o.

Finally, using (13), Fig. 9 represents the normalized real part of the image impedance for two design values of θ_o, 90° and 70° respectively. As expected, curves are equal to one only for $\theta_c = \theta_o$ and as seen, the image impedance is a pure real impedance inside the band delimited by θ_{z_1}. In addition, from Fig. 4 and Fig. 8, it is deduced that only the coupling level conditions the operating bandwidth, but from Fig. 5 and Fig. 7 it is proved that the magnitude of the frequency response depends on both, the coupling factor and the selected θ_o.

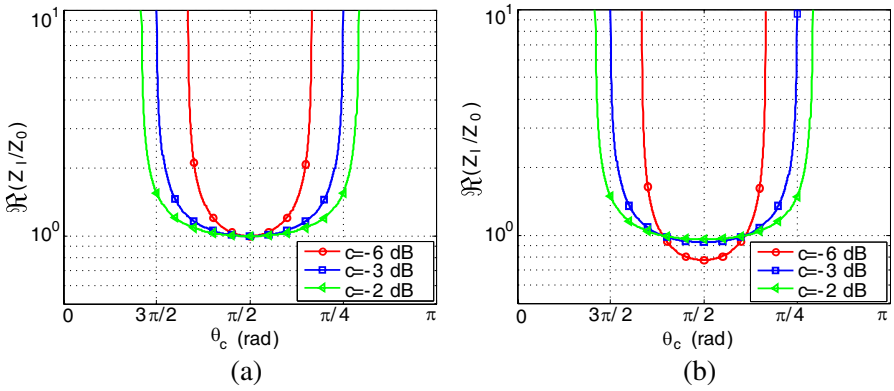

Figure 9. Normalized real part of the image impedance as a function of θ_c for two design values of θ_o, (a) 90° and (b) 70°, and several coupling factors.

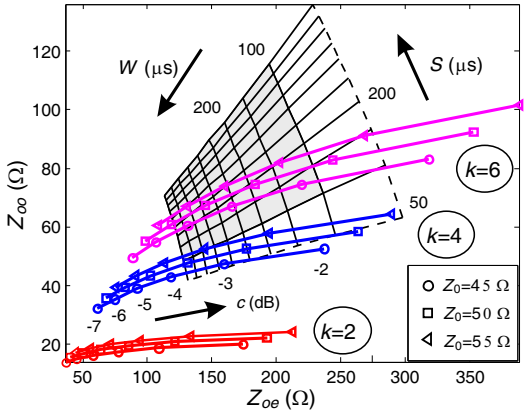

Figure 10. Achieved even and odd mode impedances as functions of the width W and spacing S on the substrate RO4350B with $\epsilon_r = 3.66$ and thickness of 30 mil. Design values of both impedances for $k = [2, 4, 6]$, $\theta_o = 90$ degrees and $Z_0 = [45, 50, 55]$ Ω are also depicted. The design values, calculated for coupling factors ranging from −7 dB to −2 dB, are labeled with circle, square and triangle marks.

3. IMPLEMENTATION AND MEASUREMENTS

In this section, to validate the theory presented in Section 2, some prototypes are fabricated and measured on Rogers 4350B substrate with relative permittivity of 3.66 and thickness of 30 mil.

Figure 10 represents, by means of [21], the achieved values of Z_{oe} and Z_{oo} when W and S range from 50 µm to 500 µm. The shaded region determines the values of impedances that are achievable using 100 µm as limit of fabrication for both, the width and spacing between conductors. This limit is a typical technical requirement for etching plastic substrates. Then, with (14), the design values of Z_{oe} and Z_{oo} are depicted for $\theta_o = 90°$, $k = [2, 4, 6]$, three reference impedances $Z_0 = [45, 50, 55]$ and several coupling factors c. In this figure, advantages by increasing the number of conductors are clearly

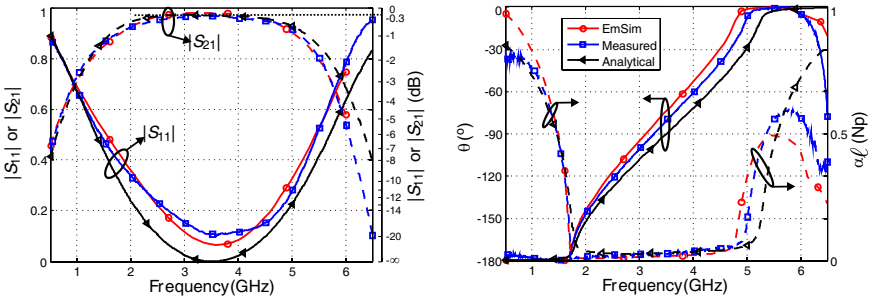

(a) (b)

Figure 11. Simulated, measured and theoretical insertion and (a) return losses and (b) dispersion diagram for a unit cell with $k = 6$, $W = 121$ µm, $S = 131$ µm, $\ell = 13.6$ mm, $\theta_o = 90°$ and $c = -3$ dB.

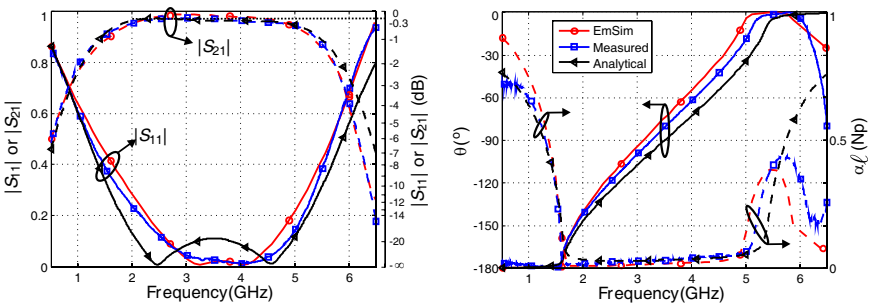

(a) (b)

Figure 12. (a) Simulated, measured and theoretical insertion and return losses and dispersion diagram for a unit cell with $k = 6$, $W = 110$ µm, $S = 100$ µm, $\ell = 13.6$ mm, $\theta_o = 63°$ and $c = -2.5$ dB.

noticeable and curves can be easily drawn for others values of such variables.

Magnitude of S_{11} and S_{21} as well as the dispersion diagram are drawn in Fig. 11 and Fig. 12 for two unit cells with $k = 6$ and using $Z_0 = 45\,\Omega$ as reference impedance. The first one is designed for $\theta_o = 90°$ with $c = -3\,\text{dB}$, while the second one has $\theta_o = 63°$ and $c = -2.5\,\text{dB}$. The value of $Z_0 = 45\,\Omega$ has been selected because, for $c = -3\,\text{dB}$, the required values of W and S are upper our limit of fabrication, as shown in Fig. 10. Furthermore, this fact it is not important because the goal here is to validate the design equations derived in previous section regardless the value of Z_0.

As seen, there is a good agreement between simulated, measured and theoretical results and curves are consistent with the theory developed in Section 2. The measured 3 dB fractional bandwidths are 127.4% and 137.1% at a center frequency of 3.5 GHz for $c = -3\,\text{dB}$ and $c = -2.5\,\text{dB}$, respectively. These results are in concordance with curves presented in Fig. 7 and Fig. 8, where it is appreciated as the higher the coupling factor, the broader the bandwidth.

Finally, three unit cells of the first design for $\theta_o = 90°$, are cascaded and measured. Fig. 13 draws the performance of such prototype, and as expected, the operating band is reduced but the frequency selectivity is improved. In this case, although the measurements fit properly the theoretical curves, greater discrepancies are appreciated at high frequencies because of the even and odd mode phase velocities dispersion. The 3 dB theoretical fractional bandwidth is 91.4% while the measured one is reduced to 61.7%. Nevertheless, it should be noted that all prototypes have been designed by means of equations given in Section 2 and there has not been any optimization process during the simulation phase. The reduction of operating

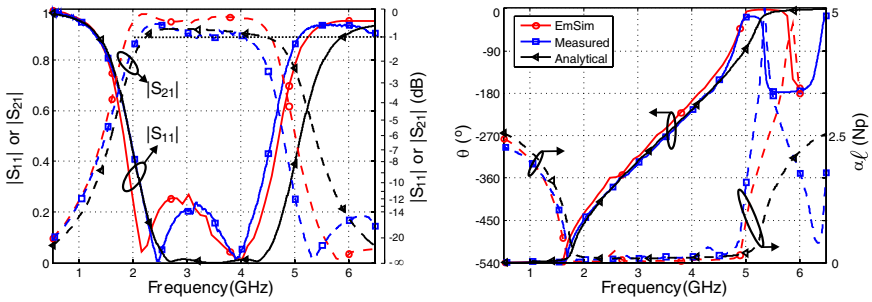

Figure 13. (a) Simulated, measured and theoretical insertion and return losses and dispersion diagram for three unit cells with $k = 6$, $W = 121\,\mu\text{m}$, $S = 131\,\mu\text{m}$, $\ell = 13.6\,\text{mm}$ and $\theta_o = 90°$.

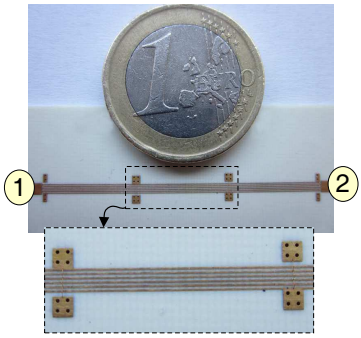

Figure 14. Photograph of three unit cells designed for $k = 6$, $\theta_o = 90°$, $Z_0 = 45\,\Omega$ and $c = -3\,\text{dB}$.

bandwidth, because microstrip is inhomogeneous, is a well known problem and can be managed by equalizing the phase velocities. A photograph of the three unit cells prototype is drawn in Fig. 14.

4. CONCLUSION

A set of novel closed-form analytical equations have been obtained in order to design wide-band bandpass filters based on wire-bonded multiconductor transmission lines. The unit cell, composed of a multiconductor TL with two of its ports short-circuited to ground has been fully characterized as a function of both, the number of conductors and the coupling factor. Hence, a bandpass filter can be designed at a particular center frequency and, its magnitude (maximally flat response or ripple response) and bandwidth can be controlled by means of the coupling level of the multiconductor structure. The validity of the design equations have been assessed by means of full-wave electromagnetic simulations and measurements. Furthermore, the good agreement between measured and theoretical results allows the design of prototypes without the need for costly electromagnetic simulations. Therefore, thanks to the theory developed, a simple and time-saving design procedure has been presented. In addition, it is important to remark that the analytical design study of the multiconductor structure carried out in this work, can be also applied to the design of hybrid rings, rat-race couplers, broadband baluns and other devices.

ACKNOWLEDGMENT

This work has been supported by the Junta de Andalucía (Spain) under Grant P09-TIC-5116 and by the Spanish Ministerio de

Ciencia e Innovación (Programa Consolider-Ingenio 2010) under Grant CSD2008-00066 ('EMET').

REFERENCES

1. Caloz, C. and T. Itoh, "Transmission line approach of left-handed (LH) materials and microstrip implementation of an artificial LH transmission line," *IEEE Trans. Antennas Propag.*, Vol. 52, No. 5, 1159–1166, May 2004.
2. Lu, W., Q. Zhu, J. Zhu, and S. Xu, "Design of bandpass filter with left-handed transmission line and highpass prototype," *Asia-Pacific Conference Proceedings Microwave Conference Proceedings*, Vol. 3, 4–7, Dec. 2005.
3. Luo, M., Z. Xu, Z. Chen, H. Nie, and L. Yu, "A novel ultra-wideband (UWB) bandpass filter using mim crlh transmission line structure," *8th International Symposium on Antennas, Propagation and EM Theory*, 690–693, Nov. 2008.
4. Kahng, S. and J. H. Ju, "Realized metamaterial CRLH bandpass filter for UHF-band WLAN with harmonics suppressed," *IEEE MTT-S International Microwave Workshop Series on Art of Miniaturizing RF and Microwave Passive Components*, 98–101, Dec. 2008.
5. Mishra, V., R. Chaudhary, K. Srivastava, and A. Biswas, "Compact two pole bandpass filter using symmetrical composite right/left handed transmission line with vias," *IEEE Asia-Pacific Conference on Applied Electromagnetics (APACE)*, 1–5, Nov. 2010.
6. Shin, E. C., C.-M. Shin, C.-H. Lee, J.-S. Park, and S. Kahng, "Low band UWB BPF using CRLH-TL metamaterial structure," *IEEE International Conference on Ultra-wideband (ICUWB)*, 499–502, Sep. 2011.
7. Caloz, C. and I. Itoh, *Electromagnetic Metamaterials: Transmission Line Theory and Microwave Applications*, Wiley-Interscience, 2006.
8. Safwat, A. M. E. and T. M. Abuelfadl, "Coupled lines from filter to composite right/left handed-cells," *Progress In Electromagnetics Research B*, Vol. 26, 451–469, 2010.
9. Abdelaziz, A. F., T. M. Abuelfadl, and O. L. Elsayed, "Realization of composite right/left-handed transmission line using coupled lines," *Progress In Electromagnetics Research*, Vol. 92, 299–315, 2009.

10. Sánchez-Martínez, J. J., E. Márquez-Segura, P. Otero, and C. Camacho-Peñalosa, "Artificial transmission line with left/right-handed behavior based on wire bonded interdigital capacitors," *Progress In Electromagnetics Research B*, Vol. 11, 245–264, 2009.
11. Myoung, S.-S., Y. Lee, and J.-G. Yook, "Bandwidth-compensation method for miniaturized parallel coupled-line filters," *IEEE Trans. Microw. Theory Tech.*, Vol. 55, No. 7, 1531–1538, Jul. 2007.
12. Lee, S. and Y. Lee, "Generalized miniaturization method for coupled-line bandpass filters by reactive loading," *IEEE Trans. Microw. Theory Tech.*, Vol. 58, No. 9, 2383–2391, Sep. 2010.
13. Ahn, H.-R., K. Min, D. Kang, S. Hong, and B. Kim, "Coupling-compensated 180° phase shift coupled-line filters terminated in arbitrary impedances," *Asia-Pacific Microwave Conference*, 649–652, Dec. 2006.
14. Lin, X. Q., P. Su, Y. Fan, and Z. B. Zhu, "Improved CRLH-TL with arbitrary characteristic impedance and its application in hybrid ring design," *Progress In Electromagnetics Research*, Vol. 124, 249–263, 2012.
15. Kuo, J.-T., C.-Y. Fan, and S.-C. Tang, "Dual-wideband bandpass filters with extended stopband based on coupled-line and coupled three-line resonators," *Progress In Electromagnetics Research*, Vol. 124, 1–15, 2012.
16. Cui, D., Y. Liu, Y. Wu, S. Li, and C. Yu, "A compact bandstop filter based on two meandered parallel-coupled lines," *Progress In Electromagnetics Research*, Vol. 121, 271–279, 2011.
17. Liu, G.-Q., L.-S. Wu, and W.-Y. Yin, "A compact microstrip rat-race coupler with modified lange and t-shaped arms," *Progress In Electromagnetics Research*, Vol. 115, 509–523, 2011.
18. Ou, W., "Design equations for an interdigitated directional coupler," *IEEE Trans. Microw. Theory Tech.*, Vol. 23, No. 2, 253–255, Feb. 1975.
19. Presser, A., "Interdigitated microstrip coupler design," *IEEE Trans. Microw. Theory Tech.*, Vol. 26, No. 10, 801–805, Oct. 1978.
20. Pozar, D., *Microwave Engineering*, 2nd edition, Wiley, New York, 1998.
21. Kirschning, M. and R. Jansen, "Accurate wide-range design equations for the frequency-dependent characteristic of parallel coupled microstrip lines," *IEEE Trans. Microw. Theory Tech.*, Vol. 32, No. 1, 83–90, Jan. 1984.